



Controlling Temperature and Relative Humidity of Ventilation Air by using a Cooling Coil and Rotary Heat Exchangers

www.ericjournal.ait.ac.th

Furugaan Ibrahim*, Surapong Chirattananon*,^{φ, #, 1}, Pattana Rakkwamsuk[†], Pipat Chaiwiwatworakul*,^{φ, #}, Surawut Chuangchote[‡], and Vu Duc Hien[†]

ARTICLE INFO

Article history:

Received 19 April 2021

Received in revised form

26 June 2021

Accepted 28 June 2021

Keywords:

Dedicated outdoor air system

Enthalpy wheel

Experiment

Sensible wheel

Simulation

ABSTRACT

Dedicated outdoor air systems (DOAS) are used to supply treated outdoor air to a cooled space. This paper focuses on a DOAS and its application in tropical climate. This DOAS is equipped with a desiccant coated Enthalpy Wheel (EW), a dehumidifying cooling coil (CC), and a sensible heat wheel (SW). A mathematical model was developed using the governing equations and validated with a TRNSYS simulation and experimental data with a coefficient of determination of 0.88 and 0.92, respectively. Simulations using the validated model showed that the DOAS configuration was applicable for the tested tropical climatic conditions. Further investigations showed that a maximum change in temperature with respect to rotational speed of SW achieved was 2.44°C, and maximum change in humidity ratio with respect to rotational speed of EW achieved was 0.38%. Also, CC showed a maximum change in temperature of 14.69°C and humidity ratio of 8.35% with respect to chilled water flow rate. Likewise, Air flow rate also showed change in temperature and humidity ratio of the supplied air.

1. INTRODUCTION

Climatic conditions in tropical regions could be hot and humid, hence air-conditioning contributes to a high portion of the total energy consumed. Although maintaining a suitable temperature and relative humidity is necessary, it is vital not to compromise the indoor air quality (IAQ) while doing so. With the increase of outdoor air (OA) requirements for buildings by 62-1989 ASHRAE standards, dedicated outdoor air system (DOAS) developments have significantly increased [1]. Realizing the importance of IAQ, many problems were highlighted in the conventional cooling systems, and decoupled systems were proposed [2]-[8]. They were proposed either as ventilation air and space air cooling system, or sensible and latent cooling system.

Various DOAS configurations are now available, and some are equipped with rotary heat exchangers. In a rotary heat exchanger, two parallel streams of (cross-flowing) air is passed through two halves of a porous rotating media. Characteristics of this media allows heat (and in some cases mass) to be exchanged between the two air streams. As such, a sensible heat exchanger wheel (SW) allows the exchange of heat only, while a desiccant coated wheel allows the exchange of mass (moisture). Then there is an enthalpy heat exchanger wheel (EW), which is a desiccant coated wheel that allows both heat and mass transfer. In addition to the rotary heat exchangers, equipment such as cooling coils (CC), run around coils, and heat pumps are also used within the DOAS assembly to improve the performance of the system such as to achieve a higher dehumidification.

Literatures show studies of various DOAS assemblies. Energy consumption of a DOAS equipped with a rotary desiccant wheel, heater and heat recovery wheel was simulated in China [9]. The study concludes that use of solar energy to heat yields the lowest energy consumption but may be not be the best economical choice due to the initial cost. Natural gas for heating was concluded to be a better choice than using electrical heater.

Multiple DOAS configurations with rotary heat exchangers and cooling coils (CC) have been modelled in TRNSYS and simulated for the tropical climate of Thailand [10]. The study concludes that a configuration of EW, SW, and run around coil around the CC shows the lowest energy consumption with a possible 19-24% reduction in total cooling load. Similar configuration was studied for the climatic condition of Singapore [11]. In this case, EW, CC, and a passive dehumidification

*The Joint Graduate School of Energy and Environment, King Mongkut's University of Technology Thonburi, Bangkok, Thailand.

^φScience and Technology Postgraduate Education and Research Development Office, Ministry of Education, Thailand.

[#]Center of Excellence on Energy Technology and Environment, Ministry of Education Thailand.

¹School of Energy, Environment and Materials, King Mongkut's University of Technology Thonburi, Bangkok, Thailand.

[†]Department of Tool and Materials Engineering, Faculty of Engineering, King Mongkut's University of Technology Thonburi, Bangkok, Thailand.

[‡]Sustainable Energy Transition program, Asian Institute of Technology, Pathum Thani, Thailand.

¹Corresponding author:

Email: surapong@jgsee.kmutt.ac.th.

component was used instead of the SW. This experimental investigation concluded that up to 30% of total cooling load could be delivered by the energy recovery wheels.

DOAS with SW, CC and EW equipped with dual wheel control system have also been studied and concluded to be the best option for all weather conditions [12]. That is, with the use of deep cooling coil for extreme weather conditions. Humidity and dry bulb temperature of the supplied air were controlled by varying the speed of EW and SW, respectively. A retrofitting simulation study to provide 100% fresh air into Intensive Care units to an existing hospital building in Egypt shows 87.50% savings in power consumption in winter and 13.53% savings in power consumption in summer [13]. In this study, like the previous study, relative humidity was controlled by the rotation speed of EW, and dry bulb temperature was controlled by the speed of SW.

In this paper, a DOAS configuration with CC, SW, and an EW was used. Objective of the study was to examine the effects of supplied ventilation air under the tropical climatic conditions of Thailand, by individually varying the rotational speed of SW and EW, by varying chilled water flow in the CC, and by varying the rate of supplied and exhausted air. Furthermore, to confirm that this DOAS configuration is a suitable model to provide outdoor air in the tropical climate and that the variable

parameters studied can be used as controls to vary the condition of the supplied air. To do so, a mathematical model was developed for CC, SW, and EW using the governing equations and simulations were carried out using MATLAB. This approach was taken because generally available simulation software's are limited when it comes to varying operational parameters (such as rotation speed of the wheel). Validation of the model was done by comparing simulated results with simulation carried out using TRNSYS and with experimental data. Results showed that the configuration was suitable for tropical climatic conditions. Moreover, controlled operating parameters allowed to control the condition of air supplied to a certain degree.

1.1 DOAS Configuration

DOAS configuration used in this study comprises of an EW, a CC, and a SW. On the supply side (refer to Figure 1) outdoor air (at ambient condition) enters the EW, where air gets cooled and dehumidified by the enthalpy recovered from the return side. Then it passes through CC where the air undergoes further cooling and dehumidification. Finally, air then undergoes reheating by the heat recovered from the return side as it passes through the SW. On the return side, the air leaving the room passes through the SW and then the EW before it leaves the system.

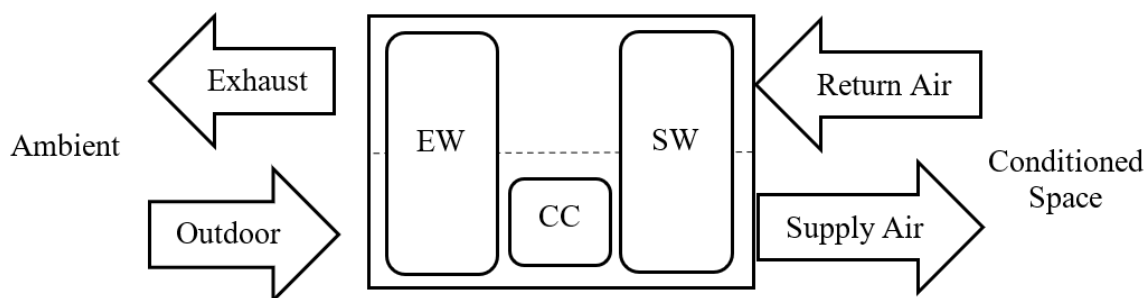


Fig. 1. DOAS configuration.

2. MATHEMATICAL MODELLING OF THE SYSTEM

Rotary heat exchangers (SW, and EW) were modelled based on the governing equations derived by Al-Ghamdi [14]. For the SW, assuming only heat transfer takes place at this, the derived governing equations for the flow region and for the matrix region by energy balance was given by Equation 1 and 2.

$$\phi \rho_g C p_g \frac{\partial T_g}{\partial t} + \phi U_g \rho_g C p_g \frac{\partial T_g}{\partial x} + h_{HT} (T_g - T_m) = 0 \quad (1)$$

$$(1 - \phi) \rho_m C p_m \frac{\partial T_m}{\partial t} = (1 - \phi) K_m \frac{\partial^2 T_m}{\partial x^2} + h_{HT} A_v (T_g - T_m) \quad (2)$$

where:

A_v : Geometrical surface volume ratio ($m^2.m^{-3}$)

$C p_g$: Specific heat capacity of air ($J.kg^{-1}.K^{-1}$)

$C p_m$: Specific heat capacity of wheel ($J.kg^{-1}.K^{-1}$)

h_{HT} : Convective heat transfer coefficient ($W.m^{-2}.K^{-1}$)

K_m : Thermal conductivity of the matrix ($W.m^{-1}.K^{-1}$)

T_g : Temperature of air (K)

T_m : Temperature of wheel (K)

t : Time steps (s)

U_g : Superficial mean gas velocity ($m.s^{-1}$)

x : Space steps (m)

ϕ : Porosity of the matrix

ρ_g : Density of air ($kg.m^{-3}$)

ρ_m : Density of the wheel ($kg.m^{-3}$)

As for the EW, since both heat and mass transfer take place at it, governing equations were derived using energy balance and mass balance. For the flow region, energy balance yielded Equation 3 and by mass balance of water vapor in the fluid region yielded Equation 4. Equation 5 and 6 was expressed for the humidity ratio in equilibrium with the matrix using air psychrometry and desiccant isotherm relationships [15]-[18]. T_0 is the temperature at which the isotherm for the desiccant was defined at, and h^* is defined as the ratio of differential heat of adsorption and specific heat of vaporization. Effect of condensation was not considered for the EW model since the model was to be used to simulate using tropical weather conditions which only requires cooling. For the Matrix region, energy balance yielded Equation 7, and by mass balance yielded Equation 8.

CC model used in this paper, was adopted from a model developed by Chirattananon [19] based on cooling coil calculations presented in HVAC Systems and Equipment in ASHRAE 2005 [20]. The model first estimates the heat transfer in the cooling coil based on the input conditions of the air and refrigerant and physical parameters of the CC. Then depending on the psychrometric conditions of air and refrigerant, the position, and the condition of the air at point where the dry section and the wet section is divided was estimated, followed by the heat transfer and area of the wet and dry section. Sum of the areas of wet and dry section areas were compared with the total area of the coil to be iterated until the areas were in an acceptable range.

$$\phi \rho_g C p_g \frac{\partial T_g}{\partial t} + \phi U_g \rho_g C p_g \frac{\partial T_g}{\partial x} + h_{HT} (T_g - T_m) = 0 \quad (3)$$

$$\phi \rho_{da} \frac{\partial \omega_g}{\partial t} + \phi \rho_{da} U_g \frac{\partial \omega_g}{\partial x} + h_{MT} (\omega_g - \omega_s) = 0 \quad (4)$$

$$\omega_s = 0.622 \frac{P_{wvs}(T_m)}{P_{atm} - P_{wvs}(T_m)} \quad (5)$$

$$\phi_s = \frac{R \bar{\omega}_m}{\bar{\omega}_{max} + (R-1) \bar{\omega}_m} \left[\frac{P_{wvs}(T_m)}{P_{wvs}(T_0)} \right]^{h^* - 1} \quad (6)$$

$$\frac{\partial T_m}{\partial t} = \frac{K_m}{\rho_m C p_m} \frac{\partial^2 T_m}{\partial x^2} + \frac{h_{HT} A_v}{(1-\phi) \rho_m C p_m} (T_g - T_m) + \frac{1}{\rho_m C p_m} \left(\begin{array}{c} \rho_{ds} h_{wv} \\ -\rho_m \left[\begin{array}{c} h_{lw}(T_m) \\ + h_{vap}(T_m) \\ - h_{ad}(T_m, \bar{\omega}_m) \end{array} \right] \end{array} \right) \frac{\partial \bar{\omega}_m}{\partial t} \quad (7)$$

$$(1-\phi) \rho_{ds} \frac{\partial \bar{\omega}_m}{\partial t} = h_{MT} A_v (\omega_g - \omega_s) \quad (8)$$

where:

- h_{ad} : Enthalpy of dry air ($J.kg^{-1}$)
- h_{MT} : Mass transfer coefficient ($kg.s^{-1}.m^{-1}$)

- h_{lw} : Enthalpy of water ($J.kg^{-1}$)
- h_{vap} : Heat of vaporization ($J.kg^{-1}$)
- h^* : Ratio of differential heat of adsorption and specific heat of vaporization
- h^* : Ratio of differential heat of adsorption and specific heat of vaporization
- P_{atm} : Atmospheric pressure (kPa)
- P_{wvs} : Saturation vapor pressure (kPa)
- R : Separation factor defining the isotherm shape
- ϕ_s : Relative Humidity (%)
- ρ_{da} : Density of dry air ($kg.m^{-3}$)
- ρ_{ds} : Density of the desiccant ($kg.m^{-3}$)
- ω_g : Humidity ratio of moist air ($kg_{wv}.kg_{da}^{-1}$)
- ω_s : Humidity ratio in equilibrium with matrix surface ($kg_{wv}.kg_{da}^{-1}$)
- $\bar{\omega}_m$: Moisture content of the desiccant ($kg_{wv}.kg_{dm}^{-1}$)
- $\bar{\omega}_{max}$: Loading of desiccant at 100% relative humidity ($kg_{wv}.kg_{dm}^{-1}$)

The major assumptions of the model included that the wheel matrix was homogenous in terms of porosity and solid structure. Exhaust and supply streams were well divided, with no intermixing. Pressure drop in the axial flow direction was negligible compared to total pressure in the system and effects of pressure drop on the thermodynamic properties of air mixture was also negligible. Lastly, heat and mass transfer coefficients were constant for supply and exhaust period. Calibration process showed that the output of the model highly depended on the thickness and the diameter of the wheel. Therefore, calibration of the model was done by adjusting the diameter and the thickness of the wheel.

2.1 Solving the System of Equations

Finite difference equations (FDE) were expressed for Equations 1 to 8. For the SW, the system of equations expressed in FDE form were linear, while FDE expressed for the system of equations of EW were non-linear. Backward finite difference expressions were used to express the FDEs for higher stability of the numerical calculations.

For the linear set of equations (*ie.* Equations 1 and 2), unknowns T_g and T_m at every point were solved by treating the system of equations as a set of simultaneous equations. As for the non-linear set of equations (*ie.* Equations 1, 3 to 8), the non-linearity arises because the present time step unknowns $\bar{\omega}_m$, ω_s , ω_g , T_g , and T_m were also functions of T_m and $\bar{\omega}_m$. Assuming the T_m and $\bar{\omega}_m$ for the dependent functions to be the same value as that of the previous time step, the system of the equations were solved as a system of linear equations. The assumed T_m and $\bar{\omega}_m$ was substituted with the calculated values, and the iterations were repeated until both sets converge. For both wheels, space steps of the FDE were a function of the depth of the wheel, and time steps was a function of the rotational speed (RPM) of the wheel. Hence the performance of the wheel (and the

system) was well represented by changes in RPM of the individual wheels. The numerical scheme grid was represented by space steps along the x-axis, and the time steps along the y-axis. Solutions of the overall grid was with a sweep along the x-direction and then moving to the next time step. MATLAB was used to solve to this numerical model, therefore from here onwards, this model will be referred to as MATLAB model in the following sections.

Figure 2 shows the flow chart of the fully assembled DOAS model. Since the wheel is in a rotational motion, at any given time, the wheel is interacting with the supply side air on one side, and the exhaust air on the other side. That is, each point of the wheel remains on the supply (exhaust) side for one half of the rotational period, and the exhaust (supply) side for the next half of the rotational period. Therefore, both supply and exhaust side were solved simultaneously before advancing in rotational time.

Initial conditions of the wheel at the supply side were the final conditions of the wheel at the exhaust side of the previous half cycle and vice versa. As for the boundary conditions, at the entrance of the wheel, condition of the fluid region and the matrix for the supply side was the condition of ambient air at the supply side. For the exhaust side, the condition of the air at the room was boundary condition. After each complete cycle, effectiveness (η) was calculated by using Equation 9. In the equation, \dot{m} is the mass flowrate of air and the $Condition$ depends on the effectiveness that is being calculated. Temperature was the condition for sensible effectiveness, humidity ratio was the condition for latent effectiveness, and enthalpy

was the condition for total effectiveness. Effectiveness values of the completed cycles were compared after each complete wheel cycle to check if the wheel has attained equilibrium and to progress to the next cycle.

$$\eta = \frac{(\dot{m}Cp_g)}{(\dot{m}Cp_g)_{max}} \frac{(Condition_{supply-air-in} - Condition_{supply-air-out})}{(Condition_{supply-air-in} - Condition_{return-air-in})} \quad (9)$$

With the description of the individual models, and the solution methodology, next step was to solve the fully assembled system as illustrated in Figure 2. Starting from the enthalpy wheel, using ambient condition ($Air_{AmbientCondition}$) as the condition of air entering at the supply side, and assuming condition of the room or cooled space ($Air_{RoomCondition}$) to be the entry condition of air at the return side ($EW_{air-return-in}$), condition of the supply side output of EW was evaluated using the EW model. This would become the condition of air entering the CC, therefor using this, the condition of air leaving the CC was evaluated. Next was to solve the SW output, this was evaluated using the CC output as the SW supply side input, and $Air_{RoomCondition}$ as the return side input. After this step, the initial assumption of $EW_{air-return-in}$ was compared with $SW_{air-return-out}$. If the values were not within an acceptable range, the calculations were repeated starting from EW model. This time the $EW_{air-return-in}$ was the $SW_{air-return-out}$ calculated in the previous step. This iteration was repeated until assumed $EW_{air-return-in}$ was equal to the calculated $SW_{air-return-out}$.

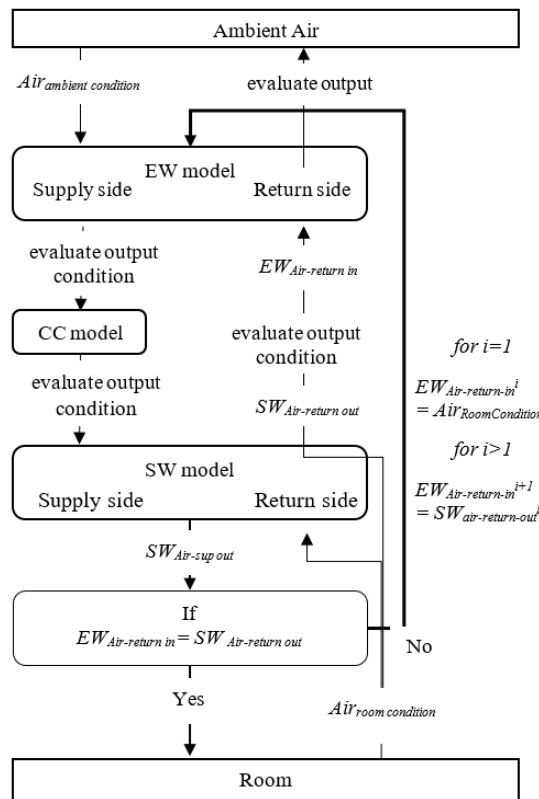


Fig. 2. Flow chart of fully configured DOAS (EW-CC-SW) model.

3. TRNSYS MODELING

Above DOAS configuration was modelled in TRNSYS 18 to compare with the mathematical model. In this part, the comparison was done with fixed operating wheel speed. Components used in the TRNSYS model have been listed in Table 1, and Figure 3 shows the TRNSYS model. Even though in an actual scenario, condition of the room will not be maintained in the above said conditions, purpose of this comparison was to see how well the model agrees to a well-known simulation model such as TRNSYS. Hence, a control volume was selected around the DOAS which includes an EW, SW and CC within the control volume. System parameters and properties were fixed, and the inputs to the control volume were the conditions of the ambient air entering at the supply side, and the conditions of the air entering to the system at the return side. For this part, both

models were simulated keeping the conditions of the return air from the room constant at 25°C and relative humidity at 50%, while TRNSYS weather data (TH-Bangkok-484550) was used as condition of ambient air entering from the supply side. Psychrometric conditions of the ambient air in this weather data file were shown in Figure 5.

Table 1. TRNSYS Components used in the model.

Component	Component Type
Enthalpy Wheel	Type667
Cooling Coil	Type52b
Sensible wheel	Type760

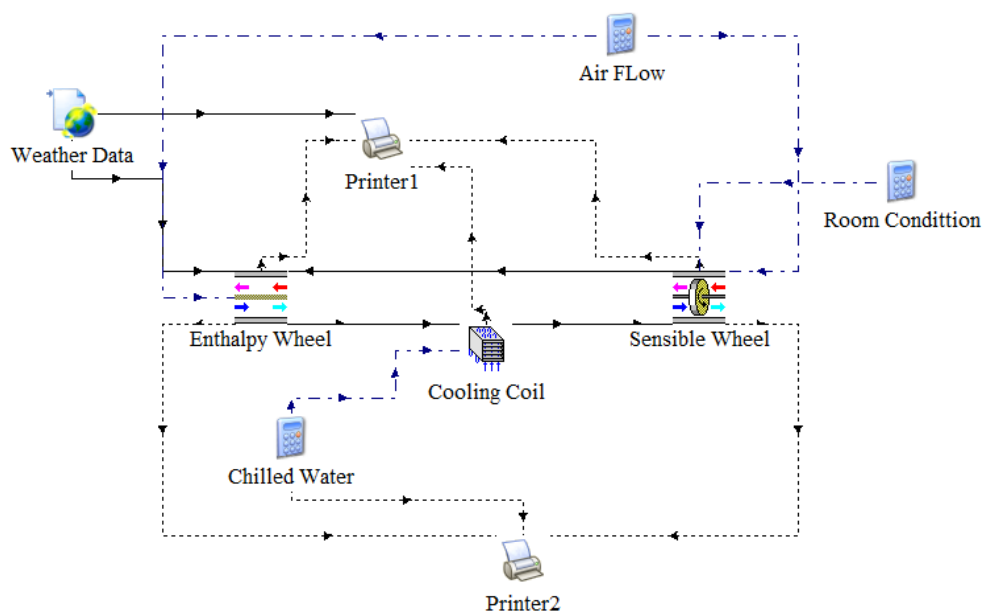


Fig. 3. TRNSYS model of DOAS.

4. EXPERIMENTAL SETUP

Experimental setup of the DOAS system was made at Bangkunjthian Campus of King Mongkut's University of Technology Thonburi, which was located at Bangkok, Thailand. Figure 4 shows the practical system which was equipped with EW, CC and SW, and sizing of the components is given in Table 2. Table 3 shows the details of the measurement devices used for data collection.

Table 2. Details of the heat exchanger wheels and cooling coil.

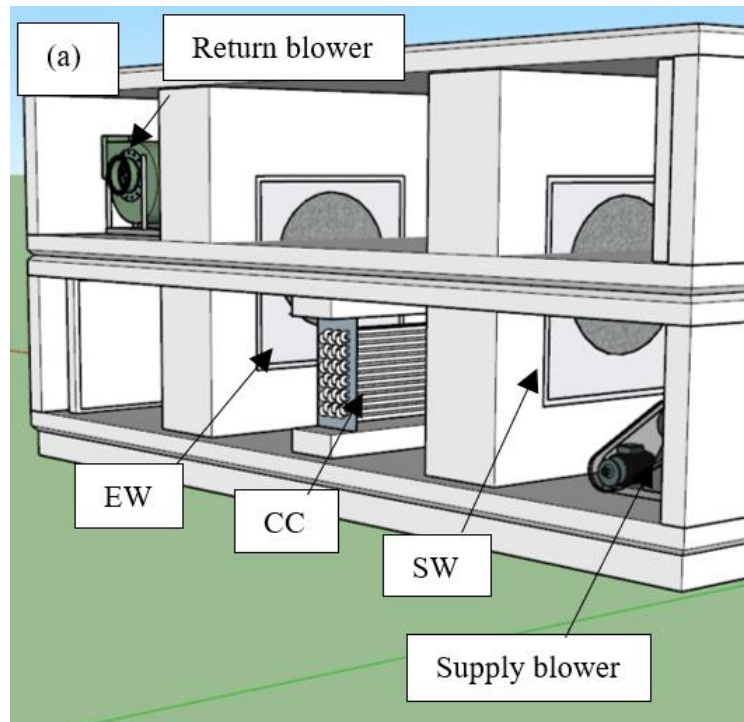
Component	Valve	Unit
Diameter of the wheels	500	mm
Depth of the wheels	295	mm
Cooling coil (length, height, depth)	890, 400, 164	mm
Number of tubes in the cooling coil	6	Nos
Number of passes in the cooling coil	12	Nos

Wheels were made from aluminum foil in a honeycomb structure, and the enthalpy wheel was coated with molecular sieve3A desiccant coating. Bry-Air wheel (model HRW500-MS200) were trimmed to the desired diameter given in Table 2 and used in a Career enclosure. The wheels and the blowers were equipped with variable speed drives. The same physical parameters were used in the MATLAB and TRNSYS model. During the experiment, conditions of the room were varied using exhaust heat from a portable air conditioner, and by boiling water in the room to get different sensible and latent loads in the room.

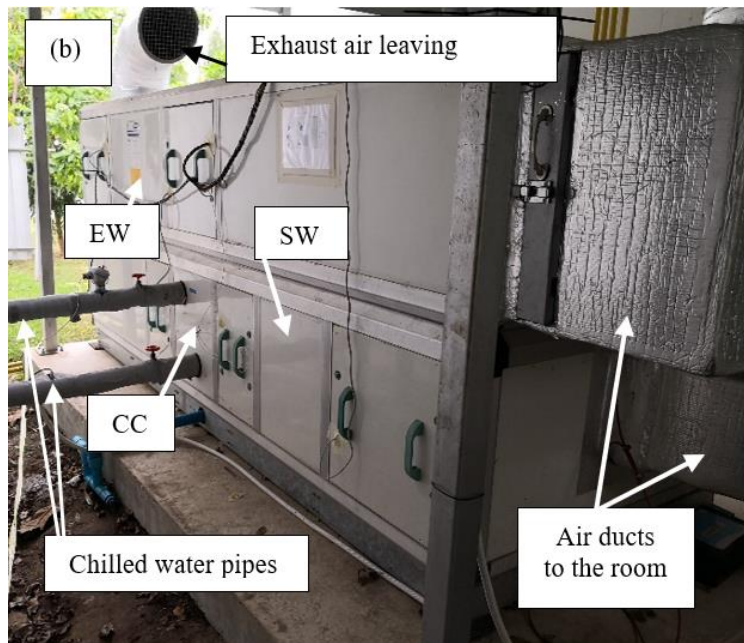
Experimented data was collected by varying chilled water flow to the CC, varying the RPM of the wheels individually, and varying the air flow rate. Since air supplied into the DOAS was the ambient air and the air exhausted into the DOAS was the air from the room, the system was subjected to varying conditions of air due to the weather. In addition to the weather conditions, and manually adjusted operating parameters mentioned

earlier, the system required roughly 30 to 45 minutes to reach steady state upon changing an operating parameter. The systems condition and ability to achieve steady was monitored live by checking the effectiveness (using Equation 9) of the of the system every minute. For the full system operation, sensors were placed at the air ducts instead of the chambers (supply chamber between EW and CC, supply chamber between CC and

SW, exhaust chamber between SW and EW... etc.) because the conducted position sensitivity tests showed high variance in measured data within chambers due to the turbulent condition of the flow within. Experimental data also showed that supply air gained heat from the blower located in the supply blower chamber resulting in a 0.23°C to 0.42°C rise in air temperature depending on the air flow rate.



(a)



(b)

Fig. 4. (a) Sectional view of DOAS and (b) DOAS setup.

Table 3. Sensors equipment’s used for data recording.

Item	Description
Model: CTV 110 KIMO instruments	Measures temperature and velocity of air Temperature measuring with an uncertainty of $\pm 0.25^{\circ}\text{C}$, and velocity measurement with an uncertainty of $\pm 0.05 \text{ ms}^{-1}$
Model: 210-R KIMO instruments	Measuring humidity and temperature Temperature measuring with an uncertainty of $\pm 0.25^{\circ}\text{C}$, and humidity measurement with an uncertainty of $\pm 1.50 \% \text{ RH}$
Model: FT440, with S-Series Low Flow meter Seametrics	For flow rate and total indicating of chilled water
Model: IN 520 LUMASENSE Technologies	IMPAC infrared thermometer

5. VALIDATION OF THE MODEL

With a mathematical model being developed, the model was validated before making any analysis using the model. Figure 5 shows the three set of weather data that was used in this paper. One set was the weather data obtained during the experiment which was during the daytime between July to September of 2018. This set was used to compare the MATLAB model with experimental data (Figure 6). Second set of weather data was from TRNSYS (TH-Bangkok-484550). This data set was used to compare the MATLAB model with TRNSYS model (Figure 7). The wider range of data available in this set of TRNSYS helped to further validate the MATLAB model and its adaptability to a full range of tropical climate. In addition to this, another

set of data was used which includes four points selected from full year weather data recorded at the weather station in Asian Institute of Technology, Thailand in 2013. These selected points were marked on Figure 5 with details give in Table 4.

Table 4. Selected points from 2013 weather data of Bangkok.

Date	Time	Temperature ($^{\circ}\text{C}$)	RH (%)
15-Jan-13	12:10	23.54	95.40
1-Mar-13	15:20	35.83	55.04
26-Mar-13	12:55	37.49	27.53
18-Dec-13	12:20	19.30	97.00

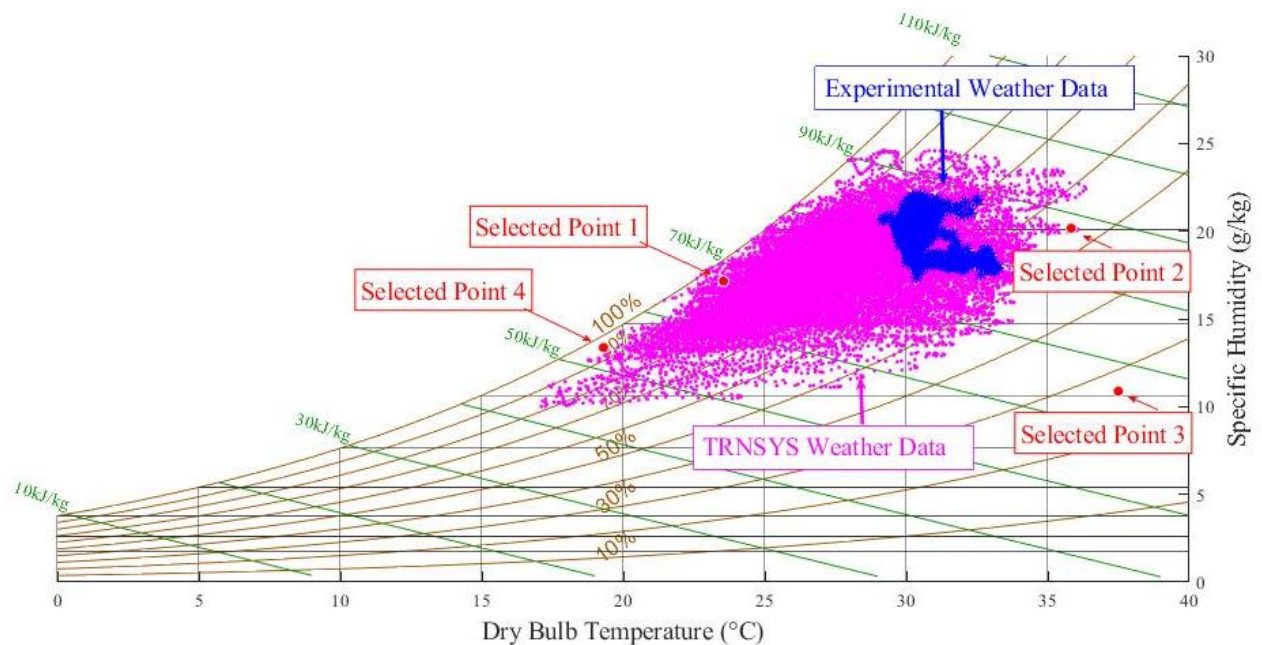


Fig. 5. Psychrometric conditions of the air in TRNSYS eather data.

Figure 6 shows total effectiveness of MATLAB model compared with measured experimental data. Data in Figure 6 encompasses recorded data with; RPM of the individual wheels varied from 1 to 25 RPM, CC water flow rate varied from 0.1 to 0.6 lps, and air flow rate varied from 300 to 400 cubic meter per hour (CMH).

Propagated error, based on the uncertainties of the measuring devices used, and the governing equations for the total effectiveness was calculated to be within $\pm 1.37\%$. Coefficient of determination (R^2) was calculated using Equation 9 to both outputs. In the equation, X was either total effectiveness from the

experiment or TRNSYS model, and Y was total effectiveness from the MATLAB model.

$$R^2 = \left(\frac{1}{N} \sum \frac{(X_i - \bar{X})(Y_i - \bar{Y})}{(\sigma_X \times \sigma_Y)} \right)^2 \quad (10)$$

Figure 6 shows that the data points lie along $y=x$ line, and the R^2 of two data sets were 0.88. Hence, MATLAB model was in good agreement with the experimental data. Do note that the total effectiveness is

higher than 1 because in addition to the heat recovered by the wheels, there is heat removed from the system by the CC. Similarly, Figure 7 shows that the MATLAB model was in good agreement with TRNSYS with an R^2 of 0.92. Also note that the span along $y=x$ line is larger for this figure because, one full year's weather data was used in this case. Hence, R^2 values, considering the percentage propagated error shows that the model is in good agreement with the TRNSYS model and experimental values.

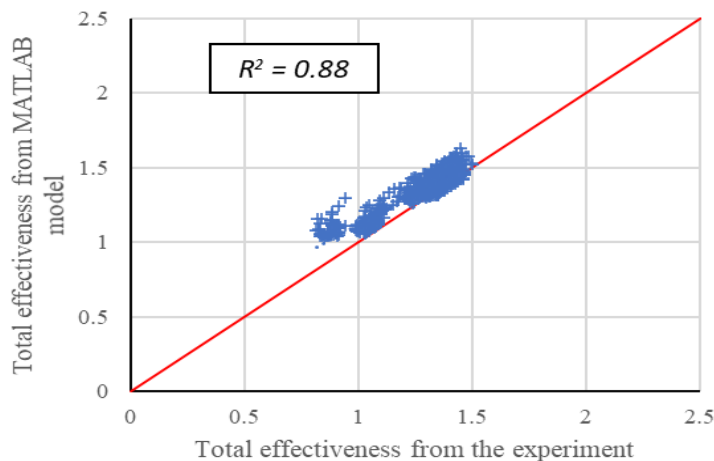


Fig. 6. MATLAB model compared with experimental data.

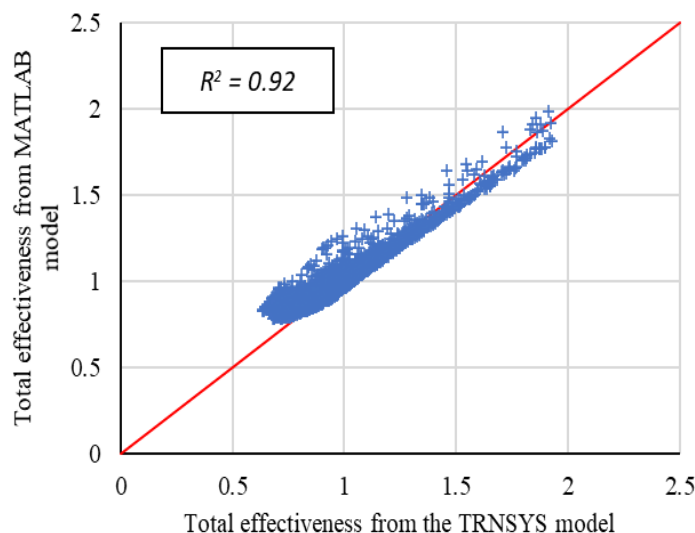


Fig. 7. MATLAB model compared with TRNSYS model.

6. SIMULATION RESULTS AND DISCUSSION

From here onwards, four selected weather conditions (in Table 4) were used to study how the system reacts to different operating conditions. As the condition of air exiting the DOAS from the supply side depends on the condition of air being vented out from the exhaust side (condition of air leaving the room), it was necessary that the exhaust air from the room be fixed to study the effects of varying other parameters. Hence, condition of the air entering to the exhaust side of the DOAS was

kept at 25°C temperature and 50% relative humidity (9g.kg⁻¹ humidity ratio).

Path taken by the supply side air at each position within the DOAS was illustrated on a psychrometric chart in Figure 8. S1 is the ambient condition of air entering the DOAS, and S2, S3, and S4 are the exit condition of air from the EW, exit condition of air from the CC, and the condition of air entering supplied to the room after it exits SW respectively. Note that all the operating parameters were kept constant for the current simulation. Results show that, for four selected weather

conditions, the system was able to supply the ventilation air between 23.90 - 24.50°C of temperature, and 8.80 - 11.60 g.kg⁻¹ humidity ratio.

Next approach was to study how the system was able to vary the condition of the supply air by varying the operating parameters of DOAS. Three scenarios were simulated in this approach. First was to vary the RPM of the EW. Figure 9 shows how the temperature and humidity ratio of the air supplied into the room varies with the RPM of EW. For all selected days, temperature and humidity ratio decreases with the increase in RPM. Gradient of the slope also decreases with the increase in RPM. For the selected condition 3,

at beginning starting from 0, a rise in temperature and humidity ratio was observed. Upon closer analysis, it was noticed that this rise was because at lower EW RPMs, supply air was undergoing cooling and humidification. This process changes to cooling and dehumidification between 4 and 5 RPM. S1–S2a and S1–S2b in Figure 8 is psychrometric process air undergoes in EW at different RPMs where RPM of S1–S2 < S1–S2a < S1–S2b. Table 5 shows the gradient of the slopes (average for all the selected conditions) in Figure 9 step wise. It should also be noted that the effect of EW RPM becomes almost negligible beyond 15 RPM.

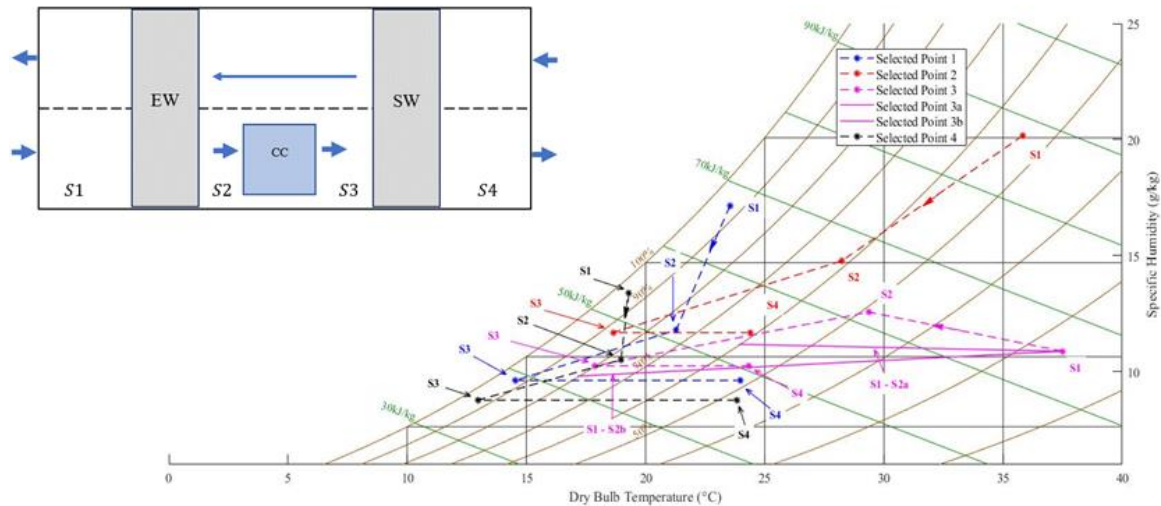


Fig. 8. System behavior for the 4 selected conditions of the year.

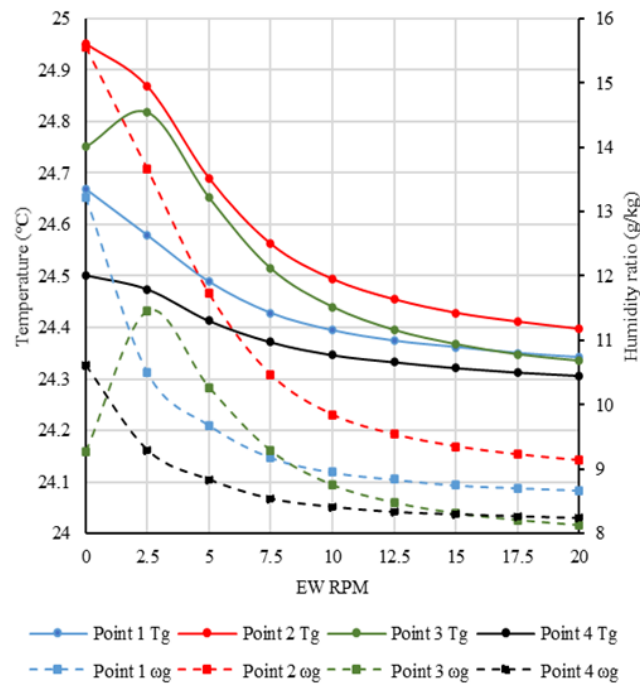


Fig. 9. Effect on temperature and humidity ratio of the supply air due to EW RPM.

Figure 10 shows the effect of varying the RPM of SW. At lower RPMs, there was an increase in the temperature with the increase of RPM, which becomes steady with the rise of RPM. No effect on humidity ratio

was noticed with the increase of SW RPM. As for the effect of temperature and humidity ratio of supply air by the flow rate, temperature of air decreases with the increase in air flow rate, while humidity ratio of supply

air increases with the increase of RPM. Table 6 shows the gradient of the slopes in Figure 10. The effect of SW

RPM was almost negligible beyond 10 RPM.

Table 5. Change in temperature and humidity ratio with respect to EW rpm.

	EW RPM ranges							
	0 - 2.5	2.5 - 5	5 - 7.5	7.5 - 10	10 - 12.5	12.5 - 15	15 - 17.5	17.5 - 20
$dT_g/dRPM$	-0.013	-0.050	-0.037	-0.020	-0.012	-0.008	-0.006	-0.004
$d\omega_g/dRPM$	-0.375	-0.440	-0.304	-0.151	-0.077	-0.048	-0.030	-0.024

Table 6. Change in temperature and humidity ratio with respect to SW rpm.

	SW RPM ranges							
	0 - 2.5	2.5 - 5	5 - 7.5	7.5 - 10	10 - 12.5	12.5 - 15	15 - 17.5	17.5 - 20
$dT_g/dRPM$	2.437	0.680	0.130	0.055	0.037	0.017	0.015	0.012
$d\omega_g/dRPM$	0.001	-0.004	-0.002	0.001	-0.001	0.000	-0.001	0.001

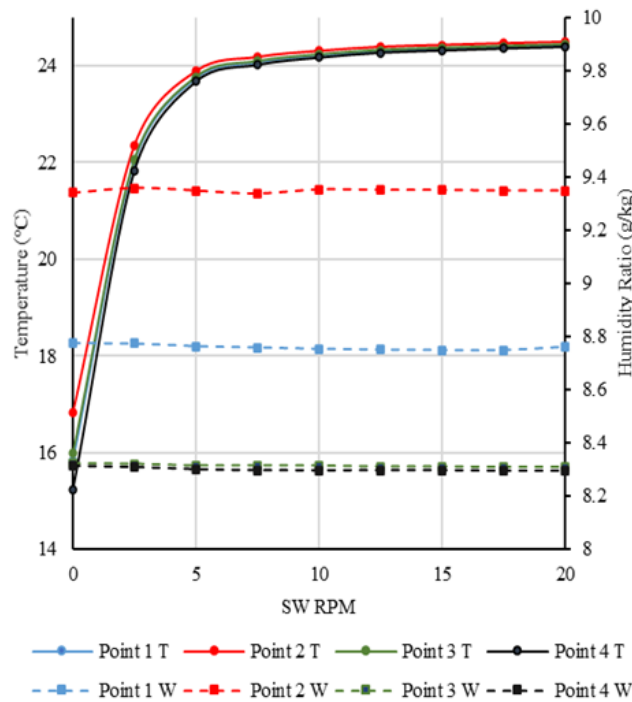


Fig. 10. Effect on temperature and humidity ratio of the supply air due to SW RPM.

Similar effect as the EW RPM was noticed by varying the chilled water flow rate of the CC as illustrated in Figure 11 and Table 7. The effect on the output temperature was higher than effect on humidity ratio, and the impact of flow rate becomes negligible beyond 0.2 lps. Lastly, Figure 12 shows the effect of varying the air flowrate on the temperature and humidity ratio of the supply air. With the increase in air flowrate, temperature of the supply air decreases, while humidity ratio of the supply air increases. The average slopes were $-8.0 \times 10^{-4} \text{ } ^\circ\text{C} \cdot \text{m}^{-3} \cdot \text{h}$ and $6.6 \times 10^{-3} \text{ g} \cdot \text{kg}^{-1} \cdot \text{m}^{-3} \cdot \text{h}$ for

dT_g/da_{flow} and $d\omega_g/da_{flow}$ respectively. Unlike other controlling parameters, effect of air flow rate on the temperature was the opposite of that on the humidity ratio. However, this control might be beneficial to provide outdoor air for a multipurpose functional space where the recommended air changes per hour might vary depending on the function of the space. Since the slopes are in opposite directions, a change airflow rate might need to be supplemented by another control measure discussed earlier.

Table 7. Change in temperature and humidity ratio with respect to CC water flow rate.

	CC water flow rate ranges					
	0 - 0.1	0.1 - 0.2	0.2 - 0.3	0.3 - 0.4	0.4- 0.5	0.5 - 0.6
dT_g/dw_{flow}	-14.699	-0.185	-0.070	-0.027	-0.023	-0.013
$d\omega_g/dw_{flow}$	-8.350	-1.357	-0.438	-0.220	-0.147	-0.095

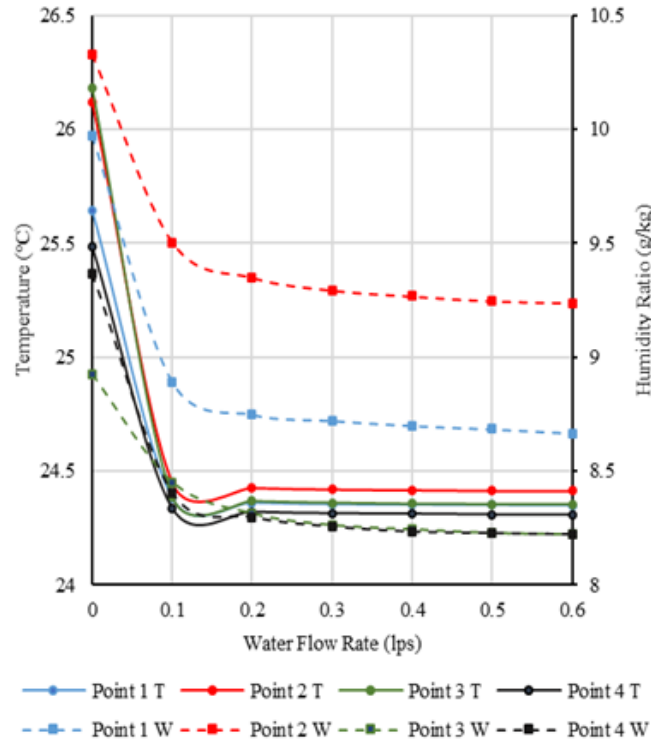


Fig. 11. Effect on temperature and humidity ratio of the supply air due to chilled water flow rate in CC.

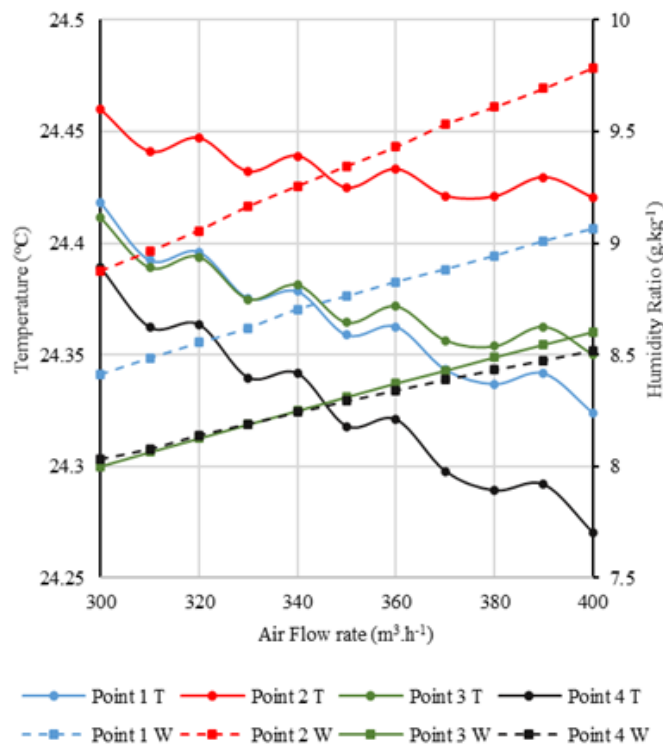


Fig. 12. Effect on temperature and humidity ratio of the supply air due to air flow rate.

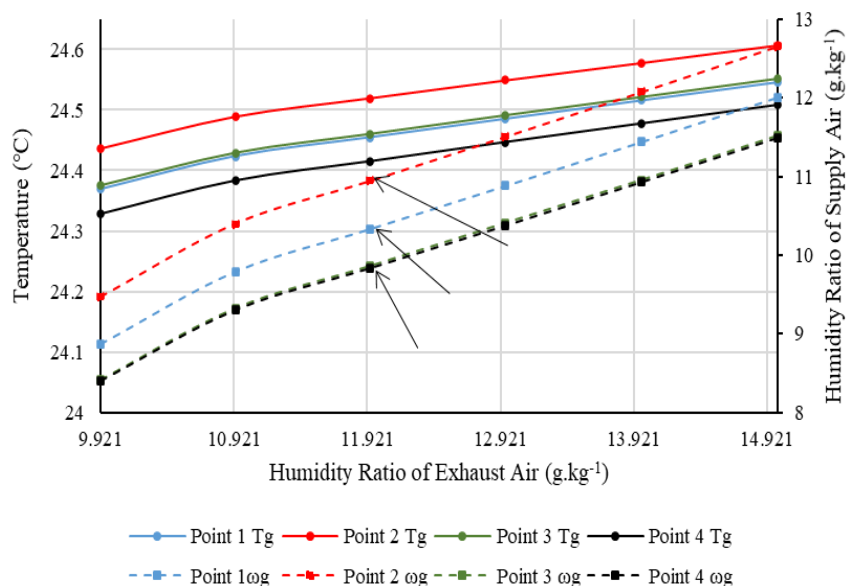


Fig. 13. Effect of exhaust air condition on the supplied air.

Final analysis of this study was to check the effect of the condition of exhaust air (which is in the room due to the cooling loads in the room) on the supply air treated by the DOAS. Assumption here was that the parallel cooling system was handling the sensible load in the space, hence keeping the air at 25°C. Figure 13 shows the condition of the air supplied for the 4 selected conditions by varying the relative humidity of the exhaust air from 50% to 75% in steps of 5%. To simplify the discussion, humidity ratio has been used as axis labels instead of relative humidity. With the slopes rather constant, for any selected point (as marked with coordinates on Figure 13), humidity ratio of the supply air (on the secondary y-axis) was lower than humidity ratio of air at the exhaust air stream (on the x-axis). Therefore, a net effect to lower the moisture content in the space was there for all the selected conditions. This was indicative that the DOAS configuration was able to meet the latent load requirements under the tested weather conditions.

Overall results showed that wheel speeds can be modulated to change the condition of the supply air;

- SW speeds can be modulated to control the temperature of the supplied air,
- EW speed can be modulated to control the humidity ratio of the supplied air,
- water flow in CC can also be used as control for temperature and humidity ratio of supplied air, and
- air flow also can be used as a control but might have to be supplemented by another control.

Results were in agreement with [12], and the simulated results showed that the system with the controls can be used in the tropical climatic conditions.

Similar system was studied in a retrofitting approach to reduce the energy consumption in an Intensive Care Unit of an existing hospital building in Egypt [13]. The simulation study showed that the system could save up to 87.15% energy savings in winter, and 13.53% energy savings in summer. As seen in this study, wheels at 0 RPM results in one condition of air

supplied by the DOAS, the study also showed that the switching the wheels off was also an operating option which showed energy savings depending on the supply and exhaust air conditions.

7. CONCLUSION

- Propagated error based on the uncertainties of the measuring devices were calculated to be within $\pm 1.37\%$, and the mathematical model (MATLAB model) was in good agreement with the experimental data (with an $R^2 = 0.88$) and TRNSYS simulation (with an $R^2 = 0.92$).
- Simulated scenarios show that the tested DOAS configuration could be used in Tropical climate and system had the potential to meet latent load requirements.
- RPM of SW could be used to control the dry bulb temperature of the supplied air and this investigation shows 2.44 as a highest change of dry bulb temperature with respect to RPM. Effect of SW RPM becomes almost negligible when it is higher than 10 RPM.
- RPM of EW could be used to control the humidity ratio of the supplied air and this investigation shows 0.38 as a highest change in humidity ratio with respect to RPM. Effect of EW RPM becomes almost negligible when it is higher than 15 RPM.
- Chilled water flow rate of CC could be used to control both dry bulb temperature and humidity ratio of the supplied air. This investigation shows $14.70^\circ\text{C.lps}^{-1}$ as a highest change in dry bulb temperature with respect to water flow rate, and $8.35 \text{ g.kg}^{-1}.\text{lbs}^{-1}$ as a highest change in humidity ratio with respect to water flow rate.
- Air flow rate also have an effect on the dry bulb temperature and humidity ratio of supplied air but have to be supplemented by other control parameters. Average change in dry bulb temperature with respect to air flow rate was $-8.0 \times 10^{-4} \text{ }^\circ\text{C.m}^{-3} \cdot \text{h}$, and average change in humidity

ratio with respect to air flow rate was at 6.6×10^{-3} $\text{g.kg}^{-1}.\text{m}^{-3}.$ H.

ACKNOWLEDGEMENT

The authors would like to express their gratitude to The Joint Graduate School of Energy and Environment (JGSEE), King Mongkut's University of Technology Thonburi and the Center of Excellence on Energy Technology and Environment (CEE), PERDO, Ministry of Higher Education, Science, Research and Innovation for the financial support provided to perform this study.

REFERENCES

- [1] Deng S., 2014. Energy benefits of different dedicated outdoor air systems configurations in various climates. MSc Thesis, University of Nebraska, Lincoln, USA (unpublished).
- [2] Coad W., 1999. Conditioning ventilation air for improved performance and air quality. *HPAC Engineering* 49-56.
- [3] Khattar M.K. and M.J. Brandemuehl. 2002. Separating the V in HVAC: A dual-path approach. *ASHRAE Journal* 44: 37-40.
- [4] Mumma S.A. and B.W. Lee. 1998. Extension of the multiple spaces concept of ASHRAE Standard 62 to include infiltration, exhaust/exfiltration, interzonal transfer, and additional short-circuit paths. *ASHRAE Transactions* 104: 1232-1241.
- [5] Scofield C.M. and N.H. Des Champs. 1993. HVAC Design for Classrooms: Divide and Conquer. *HPAC Engineering* 65(5): 53-59.
- [6] Kilkis B.I., Suntur S.R., and Sapci M., 1995. Hybrid HVAC systems. *ASHRAE Journal* 37(12): 23-28.
- [7] Mumma S.A., 2001. Overview of integrating dedicated outdoor air systems with parallel terminal systems. *ASHRAE Transactions* 107(1): 545-552.
- [8] Niu J.L., Zhang L.Z., and Zuo H.G., 2002. Energy savings potential of chilled-ceiling combined with desiccant cooling in hot and humid climates. *Energy Buildings* 34(2): 487-495.
- [9] Liu W., Lian Z., Radermacher R., and Yao Y., 2007. Energy consumption analysis on a dedicated outdoor air system with rotary desiccant wheel. *Energy* 32(9): 1749-1760.
- [10] Inklab N., Chaiwiwatworakul P., Chuangchote S., Rakkwamsuk P. and Chirarattananon S., 2015. Performance assessment of dedicated outdoorair systems for office building in Thailand. *Energy Procedia* 79: 677-684.
- [11] Murray P., Rysanek A.M., Pantelic J., Mast M., and Schlueter A., 2015. On decentralized air-conditioning for hot and humid climates: Performance characterization of a small capacity dedicated outdoor air system with built-in sensible and latent energy recovery wheels. *Energy Procedia* 78: 3471-3476.
- [12] Mumma S.A., 2001. Dedicated outdoor air-dual wheel system control requirements. *ASHRAE Transactions* 107: 147-155.
- [13] El-Maghlany W.M., ElHefni A.A., ElHelw M., and Attia A., 2017. Novel air conditioning system configuration combining sensible and desiccant enthalpy wheels. *Applied Thermal Engineering* 127: 1–15.
- [14] Al-Ghamdi A.S., 2006. Analysis of air-to-air rotary energy wheels. PhD Thesis, Russ College of Engineering and Technology, Ohio University, USA (unpublished).
- [15] Jurinak J.J. and W.M. Mitchell. 1984. Effect of matrix properties on the performance of a counter flow rotary dehumidifier. *ASME Journal of Heat and Mass Transfer* 106: 638-645.
- [16] Jurinak J.J., 1982. Open cycle solid desiccant cooling-component models and system simulations. PhD Thesis, University of Wisconsin, Madison, USA (unpublished).
- [17] Stiesch G., Klein S.A., and Mitchell J.W., 1995. Performance of rotary heat and mass exchangers. *HVAC&R Research* 1: 308-324.
- [18] Chirarattananon S., 2005. Cooling tower. In *Building for Energy Efficiency*. Building Energy Management Project, pp 366–372.
- [19] Chirarattananon, S., 2005. Holistic Approach to Calculation of Energy use in Buildings. In *Building for Energy Efficiency*. Building Energy Management Project, pp 319–383.
- [20] ASHRAE. 2005. Air-cooling and dehumidifying coils. In *HVAC Systems and Equipment*. ASHRAE.

